Unified Framework for Osmotic Energy Conversion

Oren Lavi*, Ramadan Abu-Rjal*, and Yoav Green**

Department of Mechanical Engineering, Ben-Gurion University of the Negev, Beer-Sheva, Israel

* These authors contributed equally
** Email: yoavgreen@bgu.ac.il

SUPPLEMENTAL MATERIAL

Supplemental Material Table of Contents

Notations:

Most of the derived expressions in this work will depend on the properties at the microchannel-nanochannel interfaces [such as $\overline{c}_1$ and $\overline{S}_1$, given by Eqs. (S27) and (S38) given below]. For brevity, all interfacial properties are denoted with an overbar. In a similar manner, all properties derived at $I=0$, are denoted with a hat (e.g., $\hat{\overline{c}}_1$ and $\hat{\overline{S}}_1$), such as those given in the main text [Eqs. (10) and (11)].

SI. MATHEMATICAL MODEL

Before presenting the derivation, it should be noted that the mathematical procedure utilized in this work to derive an $i-V$ and $i-j$ relations has been detailed in several of our past works. Each time, the procedure was slightly altered to account for the specific changes. Our first works that utilized this method considered a three-layered system in 2D [1] and 3D [2]. We then applied it to a one-layered system subject to a concentration gradient (with symmetric diffusion and asymmetric diffusion coefficients) [3–5], as well as to a 1D three-layered system subject to a viscosity gradient [6]. In this work, we utilize these methods to model a 3D three-layer system under a concentration gradient, with symmetric diffusion coefficients. Most of the mathematics remains unaltered.

A. Governing equations

For a system filled with a KCl(-like) saline solution with equal diffusion coefficients, $D_{\pm}=D$ and symmetric valences, $z_{\pm}=\pm z=\pm 1$, the steady-state, convectionless ion transport through a permselective medium is described by the Poisson-Nernst-Planck (PNP) equations [7–9]

$$\varepsilon_0\varepsilon_r\nabla^2\phi=-\rho_e=-F(c_+-c_-+\Sigma_s\delta_{2k})\,. \tag{S1}$$

$$-\nabla\cdot\mathbf{j}_+=\nabla\cdot\left(D\nabla c_+ +\frac{DF}{RT}c_+\nabla\phi\right)=0\,, \tag{S2}$$

$$-\nabla\cdot\mathbf{j}_-=\nabla\cdot\left(D\nabla c_- -\frac{DF}{RT}c_-\nabla\phi\right)=0\,. \tag{S3}$$

Herein, $\Re$ is the universal gas constant, T is the absolute temperature, and F is the Faraday constant, $\tilde{\varepsilon}_0$ is the permittivity of vacuum, and ε_r is the relative permittivity of the solution. Eq. (S1) is the Poisson equation for the electric potential ϕ that depends on the space charge density, ρ_e, where δ_{2k} is Kronecker's delta (for Region 2), while $k=1,2,3$ denotes each region, and $\Sigma_s>0$ is the effective excess counterion concentration in the permselective region accounting for the (negative) surface charge density, σ_s. The $\Sigma_s-\sigma_s$ relation (discussed in the main text) is given by

$$\Sigma_s=-\frac{\sigma_s\mathscr{P}}{FA}\,, \tag{S4}$$

where $\mathscr{P}$ is the perimeter, and A is the cross-sectional area (for a derivation of this $\Sigma_s-\sigma_s$ relation in cylindrical coordinates, see Appendix A of [10]). Equations (S2) and (S3) are the Nernst−Planck equations for the ionic fluxes, $\mathbf{j}_{\pm}$, for the cation and anion concentrations, c_+ and c_-, respectively. It should be noted that Σ_s has two interpretations: the normalized average excess

counterion concentration or the Duhkin number [11] (the ratio of the conductance associated with the surface charge and the conductance associated with the bulk). This parameter Σ_s is intimately linked to the transport number (which will be defined later), which is the most important proxy for the ionic selectivity of a system.

At the two ends of the system, there are two bulk reservoirs containing the same electrolyte but with different concentrations and under a potential drop of V

$$c_{\pm}(x=0)=c_{\text{left}} \quad , \quad c_{\pm}(x=\Delta_3)=c_{\text{right}} \quad , \quad \phi(x=0)=V \quad , \quad \phi(x=\Delta_3)=0 \,. \tag{S5}$$

For brevity, we define the ratio of the bulk concentrations as

$$C_r = c_{\text{right}} / c_{\text{left}} \,. \tag{S6}$$

B. Local electroneutrality, salt and electrical currents, and reduced equations

1. Local cross-section electroneutrality.

The electrical properties of the microchannels and nanochannels are different. This difference can be attributed to their size and confinement. To understand this better, one first needs to consider the electric double layer (EDL) or Debye length that forms at a charged surface when it contacts an electrolyte solution. The Debye length is defined as $\lambda_D = \sqrt{\varepsilon_0 \varepsilon_r \Re T / 2F^2 c_{\text{bulk}}}$ where c_{bulk} is either c_{left} or c_{right}. This length, which typically ranges from 0.1 nm (at very high concentrations) to 100 nm (at very low concentrations), characterizes the length where the effects of the surface charge density are non-negligible. In a microchannel, the EDL is substantially smaller than all other lengths (wherein $\lambda_D \ll L_k, W_k, H_k$), such that the response of the microchannel can be considered to be independent of the surface charge entirely. In contrast, within the nanochannel, one can have that $\lambda_D \gg H_k$ (or W_k) but $\lambda_D \ll L_k$. When $\lambda_D \gg H_k$, the top and bottom EDLs overlap, leading to a region where the effects of the surface charge [through Eq. (S4)] span the entire region. Thus, in the microchannel, we are Σ_s independent, while in the nanochannel, we are Σ_s dependent. This leads to an almost discontinuous jump of various properties at the two microchannel-nanochannel interfaces located at $x = \Delta_1, \Delta_2$. These jumps are discussed further below (as well as in our past works [4,5]).

Importantly, the fact that $\lambda_D \ll L_{k=1,2,3}$ results in a key simplification – this is the existence of local and cross-sectional electroneutrality. As we have already stated, in the microchannel, one can assume that the effects of the surface charge density are negligible, such that Eq. (S1) can be reduced to a simplified form of $\rho_e = F(c_+ - c_-) = 0$ [2,12]. Since this equation holds at every point, we can require local electroneutrality such that

$$c_{k=1,3} = c_+ = c_- . \tag{S7}$$

In the charged nanochannel, an alternative approach is needed. If one considers a cross-sectional averaging procedure, which is allowed so long as $L_2 \gg A^{1/2}$ (or $L_2 \gg \sqrt{H_2 W_2}$), then σ_s gives rise to an excess average counterion concentration, given by Eq. (S4). If $\lambda_D \ll L_2$, then one can still require that $\rho_e = 0$. However, now it should be remembered that $\rho_e = F(c_+ - c_- - \Sigma_s)$. The requirement that $\rho_e = 0$ at every cross-section yields

$$c_{2-} = c_2 \quad , \quad c_{2+} = c_{2-} + \Sigma_s = c_2 + \Sigma_s . \tag{S8}$$

2. *Salt current and electric current.*

The salt current density j and the electric current density i are defined as

$$\mathbf{j} \equiv \mathbf{j}_+ + \mathbf{j}_- \quad , \quad \mathbf{i} \equiv F(\mathbf{j}_+ - \mathbf{j}_-) . \tag{S9}$$

If one assumes the current density to be uniform across the cross-section, the 3D salt and electrical currents are given by

$$J = jA \quad , \quad I = iA , \tag{S10}$$

where A is the nanochannel cross-section, in this case, a rectangle, $A = H_2 W_2$. However, the assumption of a particular cross-sectional geometry can be relaxed, and the more general approach utilizing A can be leveraged.

3. *Reduced equations in Regions 1 and 3.*

Inserting Eq. (S7) into Eqs. (S2) and (S3), and accounting for Eq. (S9) [adding and subtracting Eqs. (S2)-(S3)], we find a reduced set of equations for the salt current density and electrical current density in regions $k = 1,3$

$$-\nabla \cdot \mathbf{j} = 2D\nabla^2 c_k = 0 \quad \text{where} \quad \mathbf{j} = -2D\nabla c_k , \tag{S11}$$

$$-\nabla \cdot \mathbf{i} = 2\frac{DF}{V_{\text{th}}} \nabla \cdot (c_k \nabla \phi_k) = 0 \quad \text{where} \quad \mathbf{i} = -2\frac{DF}{V_{\text{th}}} c_k \nabla \phi_k . \tag{S12}$$

where $V_{\text{th}} = \Re T / F$ is the thermal potential.

4. *Reduced equations in Region 2.*

Since we have already considered cross-sectional electroneutrality, only 1D changes in the longitudinal directions need to be considered. In Region 2, we insert Eq. (S8) into Eqs. (S2) and (S3), resulting in the following 1D fluxes

$$-j_+ = Dc_{2,x} + \frac{D}{V_{\text{th}}}(c_2 + \Sigma_s)\phi_{2,x}, \quad -j_- = Dc_{2,x} - \frac{D}{V_{\text{th}}} c_2 \phi_{2,x} , \tag{S13}$$

The subscript of the comma and x denotes a derivative by x. Inserting these two equations into Eq. (S9), yields the simplified equations [1–5]

$$\frac{DF}{V_{\text{th}}}(2c_2+\Sigma_s)\phi_{2,x}=-i\,, \tag{S14}$$

$$2Dc_{2,x}+\frac{D}{V_{\text{th}}}\Sigma_s\phi_{2,x}=-j\,. \tag{S15}$$

C. Boundary conditions

Equations (S11)-(S12) and (S14)-(S15) will be solved for each region, subject to the following boundary conditions (BCs), in addition to those specified in Eq. (S5).

Regions 1 and 3. On all the microchannel walls, we require no flux. Mathematically, this can be translated to

$$\mathbf{n}\cdot\mathbf{j}_{\pm}=0\ \ ,\ \mathbf{n}\cdot\nabla\phi=0\,, \tag{S16}$$

which can be further simplified to

$$\mathbf{n}\cdot\nabla c=0\ \ ,\ \mathbf{n}\cdot\nabla\phi=0\,, \tag{S17}$$

where $\mathbf{n}$ is the unit vector normal to the surface. Explicitly, for Regions 1 and 3 ($k=1,3$), we require that

$$c_{k,y}(y=0,H_k)=c_{k,z}(z=\pm\tfrac{1}{2}W_k)=0\,, \tag{S18}$$

$$\phi_{k,y}(y=0,H_k)=\phi_{k,z}(z=\pm\tfrac{1}{2}W_k)=0\,. \tag{S19}$$

For simplicity, and to ensure conservation of total fluxes across the microchannel-nanochannel interfaces located at $x=\Delta_1,\Delta_2$, we require that the salt current and electrical current densities [Eqs. (S11)-(S12)] are uniformly distributed at these interfaces

$$c_{k,x}=\begin{cases}-\frac{1}{2D}j & ,y\in[0,H_2],z\in[-\frac{1}{2}W_2,\frac{1}{2}W_2]\\ 0 & ,else\end{cases}, \tag{S20}$$

$$c_k\phi_{k,x}=\begin{cases}-\frac{1}{2}\frac{V_{\text{th}}}{DF}i & ,y\in[0,H_2],z\in[-\frac{1}{2}W_2,\frac{1}{2}W_2]\\ 0 & ,else\end{cases} \tag{S21}$$

Region 2. Note that in the derivation of Eqs. (S14)-(S15), which utilized cross-sectional averaging, the boundary conditions $\varepsilon_0\varepsilon_r\mathbf{n}\cdot\nabla\phi=-\sigma_s$ (through Σ_s) and $\mathbf{n}\cdot\mathbf{j}_{\pm}=0$ have already been satisfied – see Refs. [10,13] for a detailed derivation of Eq. (S4). As such, only the BCs at $x=\Delta_1,\Delta_2$ need to be provided. These BCs will be provided shortly.

SII. SOLUTION DERIVATION

In this section, we solve the governing equations in all three regions, subject to their appropriate boundary conditions. From these solutions, we will derive the two master equations presented in this work.

A. Regions 1 and 3

1. Concentrations

We find the concentration distributions in both Regions 1 and 3 using the standard separation of variables procedure, as used in our past works [1,2,14,15]. This involves solving Eq. (S11) and the BCs specified in Eqs. (S5), (S18), and (S20), which yields

$$\begin{aligned} c_1(x,y,z) &= c_{\text{left}} - \frac{J}{2DW_1H_1}x \\ &- \frac{J}{DW_1H_1}\left\{\frac{1}{H_2}\sum_{n=1}^{\infty}\frac{\sin[\lambda_n^{(1)}H_2]}{[\lambda_n^{(1)}]^2\cosh[\lambda_n^{(1)}L_1]}\cos[\lambda_n^{(1)}y]\sinh[\lambda_n^{(1)}x]\right. \\ &+ \frac{2}{W_2}\sum_{m=1}^{\infty}\frac{\sin[\frac{1}{2}\gamma_m^{(1)}W_2]}{[\gamma_m^{(1)}]^2\cosh[\gamma_m^{(1)}L_1]}\cos[\gamma_m^{(1)}z]\sinh[\gamma_m^{(1)}x] \\ &\left.+ \frac{4}{W_2H_2}\sum_{n,m=1}^{\infty}\frac{\sin[\lambda_n^{(1)}H_2]\sin[\frac{1}{2}\gamma_m^{(1)}W_2]}{\kappa_{n,m}^{(1)}\lambda_n^{(1)}\gamma_m^{(1)}\cosh[\kappa_{n,m}^{(1)}L_1]}\cos[\lambda_n^{(1)}y]\cos[\gamma_m^{(1)}z]\sinh[\kappa_{n,m}^{(1)}x]\right\} \end{aligned}, \tag{S22}$$

and

$$\begin{aligned} c_3(x,y,z) &= c_{\text{right}} + \frac{J}{2DW_3H_3}(\Delta_3 - x) \\ &+ \frac{J}{DW_3H_3}\left\{\frac{1}{H_2}\sum_{n=1}^{\infty}\frac{\sin[\lambda_n^{(3)}H_2]}{[\lambda_n^{(3)}]^2\cosh[\lambda_n^{(3)}L_3]}\cos[\lambda_n^{(3)}y]\sinh[\lambda_n^{(3)}(\Delta_3 - x)]\right. \\ &+ \frac{2}{W_2}\sum_{m=1}^{\infty}\frac{\sin[\frac{1}{2}\gamma_m^{(3)}W_2]}{[\gamma_m^{(3)}]^2\cosh[\gamma_m^{(3)}L_3]}\cos[\gamma_m^{(3)}z]\sinh[\gamma_m^{(3)}(\Delta_3 - x)] \\ &\left.+ \frac{4}{W_2H_2}\sum_{n,m=1}^{\infty}\frac{\sin[\lambda_n^{(3)}H_2]\sin[\frac{1}{2}\gamma_m^{(3)}W_2]}{\kappa_{n,m}^{(3)}\lambda_n^{(3)}\gamma_m^{(3)}\cosh[\kappa_{n,m}^{(1)}L_3]}\cos[\lambda_n^{(3)}y]\cos[\gamma_m^{(3)}z]\sinh[\kappa_{n,m}^{(3)}(\Delta_3 - x)]\right\} \end{aligned}, \tag{S23}$$

where the eigenvalues are defined by

$$\lambda_n^{(k)} = \frac{\pi n}{H_k}, \quad \gamma_m^{(k)} = \frac{2\pi m}{W_k}, \quad \kappa_{n,m}^{(k)} = \sqrt{[\lambda_n^{(k)}]^2 + [\gamma_m^{(k)}]^2}, \quad k = 1,3, \tag{S24}$$

2. Electric potential

The 3D electrical potential distribution follows from Eq. (S12) and the BCs in Eqs. (S5), (S19), and (S21). We find that

$$\phi_1 = \frac{V_{\text{th}}}{F}\frac{i}{j}\ln\left(\frac{c_1}{c_{\text{left}}}\right) + V = \frac{V_{\text{th}}}{F}\frac{I}{J}\ln\left(\frac{c_1}{c_{\text{left}}}\right) + V, \tag{S25}$$

$$\phi_3 = \frac{V_{\text{th}}}{F}\frac{i}{j}\ln\left(\frac{c_3}{c_{\text{right}}}\right) = \frac{V_{\text{th}}}{F}\frac{I}{J}\ln\left(\frac{c_3}{c_{\text{right}}}\right). \tag{S26}$$

It should be noted that the solutions for Region 1 [Eqs. (S22) and (S25)] and the solutions for Region 3 [Eqs. (S23) and (S26)] are very similar to the expressions previously derived in Ref. [2] for the case of symmetric concentrations ($c_{\text{right}} = c_{\text{left}}$).

3. Resistances

In the following, we use the values of the concentration at the two interfaces, located at $x = \Delta_1$ and $x = \Delta_2$, on the central axis (i.e., $y = z = 0$). These are termed the interfacial concentrations and are denoted by

$$\overline{c}_1 = c_1(\Delta_1, 0, 0) = c_{\text{left}} - \frac{J}{2D}\frac{\Sigma R_1}{\rho_{res}}, \quad \overline{c}_3 = c_3(\Delta_2, 0, 0) = c_{\text{right}} + \frac{J}{2D}\frac{\Sigma R_3}{\rho_{res}}. \tag{S27}$$

Here, $\Sigma R_{k=1,3}$ represents the total electrical resistances associated with the respective microchannels, and $\rho_{res} = \Re T / F^2 D c_{\text{bulk}}$ is the local ionic resistivity. Here, we have defined the resistivity to depend on a concentration we denote as c_{bulk}, where c_{bulk} is either c_{left} or c_{right}. In each microchannel, the resistance can be divided into two contributions such that

$$R_{k=1,3} = \rho_{res}\frac{L_k}{W_k H_k}, \quad R_{\text{FF},k=1,3} = 2\rho_{res}\overline{f}_k, \quad \Sigma R_{k=1,3} = R_k + R_{\text{FF},k}. \tag{S28}$$

The first term, $R_{k=1,3}$, is the geometric contribution associated with a cuboidal resistor, and the second term, $R_{\text{FF},k=1,3}$, is the field-focusing contribution. The $\overline{f}_k$ functions represent the contributions of the focusing of the field lines from the large 3D microchannel into the much smaller nanochannel, which we naturally term the field-focusing resistances. By inserting $x = \Delta_{1,2}$ and $y = z = 0$ into the concentration distributions [Eqs. (S22)-(S23)], we obtain the $\overline{f}_{k=1,3}$ functions,

$$\overline{f}_{k=1,3} = \frac{1}{W_k H_k}\left\{\frac{1}{H_2}\sum_{n=1}^{\infty}\frac{\sin[\lambda_n^{(k)} H_2]}{[\lambda_n^{(k)}]^2}\tanh[\lambda_n^{(k)} L_k] + \frac{2}{W_2}\sum_{m=1}^{\infty}\frac{\sin[\frac{1}{2}\gamma_m^{(k)} W_2]}{[\gamma_m^{(k)}]^2}\tanh[\gamma_m^{(k)} L_k] + \frac{4}{W_2 H_2}\sum_{n,m=1}^{\infty}\frac{\sin[\lambda_n^{(k)} H_2]\sin[\frac{1}{2}\gamma_m^{(k)} W_2]}{\kappa_{n,m}^{(k)}\lambda_n^{(k)}\gamma_m^{(k)}}\tanh]\kappa_{n,m}^{(k)} L_k]\right\}. \tag{S29}$$

This $\overline{f}_k$ expression has been investigated in several of our past works [14–17], including our very recent work [18], where we derived the expression for $\overline{f}_k$ an arbitrary geometry (and not just the rectangular geometry considered in this work).

B. Region 2 and the $i-j$ relation

In contrast to Regions 1 and 3, where explicit distributions for concentration and potential were derived, in Region 2, such a solution is not attainable. Instead, as we will shortly demonstrate, by manipulating the equations within Region 2, and accounting for the interfacial concentrations in Regions 1 and 3, an algebraic $i-j$ relationship will be uncovered.

Isolating $\phi_{2,x}$ from Eq. (S14) and inserting it into Eq. (S15) yields, after rearranging, a separable differential equation for c_2 (see [1–5] for a detailed derivation of this equation)

$$\frac{2(2c_2+\Sigma_s)}{i\Sigma_s - Fj(2c_2+\Sigma_s)}c_{2,x} = \frac{1}{FD}. \tag{S30}$$

Equation (S30) can be integrated over the domain $[\Delta_1,\Delta_2]$, yielding

$$\left\{c_2 + \frac{i\Sigma_s}{2Fj}\ln[i\Sigma_s - Fj(2c_2+\Sigma_s)]\right\}_{\bar{c}_2(\Delta_1)}^{\bar{c}_2(\Delta_2)} = x\Big|_{\Delta_1}^{\Delta_2} = -\frac{jL_2}{2D}. \tag{S31}$$

The concentrations at the two ends of the nanochannels, $\bar{c}_2(\Delta_1)$ and $\bar{c}_2(\Delta_2)$, are still not known. We shall now derive them by relating them to the interfacial concentrations $\bar{c}_{1,3}$ [Eq. (S27)].

To find these concentrations, we utilize the electrochemical potential μ of the positive and negative species, defined as

$$\mu_\pm = \Re T\ln c_\pm \pm F\phi. \tag{S32}$$

It can readily be observed that the fluxes $\mathbf{j}_+$ and $\mathbf{j}_-$ are gradients of these potentials

$$\mathbf{j}_\pm = -\frac{D}{\Re T}c_\pm\nabla\mu_\pm. \tag{S33}$$

If the fluxes are continuous at the interface, so too are the electrochemical potentials, such that $\mu_{1\pm}(\Delta_1)=\mu_{2\pm}(\Delta_1)$ and $\mu_{2\pm}(\Delta_2)=\mu_{3\pm}(\Delta_2)$. Note that these relations constitute four separate BCs. In the following paragraph, we will use two BCs, and the remaining two will be utilized later in the derivation of the current-voltage response when we account for the Donnan potential drops.

It is useful to consider the sum of the positive and negative electrochemical potentials

$$\mu = \mu_+ + \mu_- = \Re T\ln(c_+c_-). \tag{S34}$$

Since μ_+ and μ_- are each continuous at $x=\Delta_1$ and $x=\Delta_2$, so is μ. Equation (S34) can be further simplified by removing the log function and requiring that c_+c_- is continuous

$$(c_{1+}c_{1-})_{x=\Delta_1} = (c_{2+}c_{2-})_{x=\Delta_1}, \quad (c_{2+}c_{2-})_{x=\Delta_2} = (c_{3+}c_{3-})_{x=\Delta_2}. \tag{S35}$$

Utilizing the relation for the concentrations at Region 2 [Eq. (S8)] and the known interfacial concentrations [Eqs. (S27)] leads to

$$\bar{c}_1^2 = \bar{c}_2(\Delta_1)[\bar{c}_2(\Delta_1) + \Sigma_s] \ , \ \bar{c}_3^2 = \bar{c}_2(\Delta_2)[\bar{c}_2(\Delta_2) + \Sigma_s] . \tag{S36}$$

Each quadratic equation has two roots. However, since the concentration cannot be negative, we take the positive roots given by

$$\bar{c}_2(\Delta_1) = -\tfrac{1}{2}\Sigma_s + \bar{S}_1 \ , \ \bar{c}_2(\Delta_2) = -\tfrac{1}{2}\Sigma_s + \bar{S}_3 , \tag{S37}$$

where

$$\bar{S}_1 = \tfrac{1}{2}\sqrt{\Sigma_s^2 + 4\bar{c}_1^2} \ , \ \bar{S}_3 = \tfrac{1}{2}\sqrt{\Sigma_s^2 + 4\bar{c}_3^2} . \tag{S38}$$

Inserting $c_2(\Delta_1)$ and $c_2(\Delta_2)$ into Eq. (S31), and accounting for the Ohmic resistance of the nanochannel R_2, given by

$$R_{\text{nano}} = R_2 = \rho_{res}\frac{L_2}{A} = \rho_{res}\frac{L_2}{H_2 W_2} , \tag{S39}$$

yields the following $i-j$ relation

$$\Lambda(i,j) = \frac{\Sigma_s i}{2Fj}\ln\left(\frac{i\Sigma_s - 2jF\bar{S}_3}{i\Sigma_s - 2jF\bar{S}_1}\right) + (\bar{S}_3 - \bar{S}_1) + \frac{jAR_2}{2D\rho_{res}} = 0 . \tag{S40}$$

This expression provides a constraint on the salt current and electrical current densities. For simplicity, we call it the $\Lambda(i,j)$ function, or, in short, the $i-j$ relation. This is the first of the two master equations derived in this work.

C. Current-voltage relation

The voltage drop, V, across the system is comprised of the potential drops over the three regions, $\Delta\phi_{k=1,2,3}$, and the two Donnan potential drops at the two interfaces at $x = \Delta_1, \Delta_2$ ($\Delta\phi_{D,1-2}$ and $\Delta\phi_{D,2-3}$, respectively) [2], such that

$$-V = \Delta\phi = \Delta\phi_1 + \Delta\phi_{D,1-2} + \Delta\phi_2 + \Delta\phi_{D,2-3} + \Delta\phi_3 . \tag{S41}$$

The potential drops in Regions 1 and 3 are calculated via the respective potential distributions [Eqs. (S25) and (S26), respectively], and are, respectively, given by

$$\Delta\phi_1 = \phi_1(x=\Delta_1) - \phi_1(x=0) = \frac{V_{\text{th}}}{F}\frac{i}{j}\ln\left(\frac{\bar{c}_1}{c_{\text{left}}}\right), \tag{S42}$$

$$\Delta\phi_3 = \phi_3(x=\Delta_3) - \phi_3(x=\Delta_2) = -\frac{V_{\text{th}}}{F}\frac{i}{j}\ln\left(\frac{\bar{c}_3}{c_{\text{right}}}\right). \tag{S43}$$

The potential drop in Region 2 is calculated by integrating Eq. (S15). This yields,

$$\Delta\phi_2 = \frac{V_{\text{th}}}{\Sigma_s}\left(2S_3 - 2S_1 + \frac{jAR_2}{D\rho_{res}}\right). \tag{S44}$$

The Donnan potential drops can be calculated using the two remaining electrochemical potential BCs. Using the positive terms

$$\mu_{1+}(\Delta_1)=\mu_{2+}(\Delta_1)\ ,\ \mu_{2+}(\Delta_2)=\mu_{3+}(\Delta_2)\,, \tag{S45}$$

we obtain

$$\Delta\phi_{D,1-2}=-V_{\rm th}\ln\left[\frac{\bar{c}_2(\Delta_1)+\Sigma_s}{\bar{c}_1}\right],\quad \Delta\phi_{D,2-3}=V_{\rm th}\ln\left[\frac{\bar{c}_2(\Delta_2)+\Sigma_s}{\bar{c}_3}\right]. \tag{S46}$$

By inserting Eqs. (S42)-(S44), and (S46) into Eq. (S41), we find the relation between the potential drop, V, and the two current densities (i and j)

$$V(i,j)=V_{\rm th}\left[\frac{i}{Fj}\ln\left(\frac{1}{C_r}\frac{\bar{c}_3}{\bar{c}_1}\right)+\ln\frac{\bar{c}_3}{\bar{c}_1}+\ln\frac{\Sigma_s+2\bar{S}_1}{\Sigma_s+2\bar{S}_3}+2\frac{\bar{S}_3-\bar{S}_1}{\Sigma_s}+\frac{jAR_2}{D\rho_{res}\Sigma_s}\right]. \tag{S47}$$

This $i-V$ equation, given in the main text, is the second master equation derived in this work.

SIII. SUPPLEMENTAL DISCUSSIONS

A. Limiting and overlimiting currents

1. Limiting currents

Due to the selective ion transport through the nanochannel, concentration gradients form in the two different microchannels. In particular, the concentrations at the two microchannel-nanochannel interfaces vary [7]. Namely, one interface becomes more depleted, while the other interface becomes more enriched. The minimal concentration at the depleted interface [either interfacial concentration $\bar{c}_1$ or $\bar{c}_3$, Eq. (S27)] can be achieved is zero. This occurs when the salt current reaches its maximal value (in the absolute sense) or its limiting value given by

$$J_{\rm lim-1}=2Dc_{\rm left}\frac{\rho_{res}}{\Sigma R_1}\ ,\ J_{\rm lim3}=-2Dc_{\rm right}\frac{\rho_{res}}{\Sigma R_3}\,. \tag{S48}$$

In order to find the limiting electrical current, one needs to utilize the $i-j$ relation [Eq. (S40)]. In most works that discussed the limiting currents, one will typically find that J's in Eq. (S48) are replaced by I's. The reason that such an exchange is allowed is that the limiting current is typically investigated in ideally selective systems, where $\Sigma_s \gg \max(c_{\rm left},c_{\rm right})$, and only the counterions (here, positive species) are transported such that $I=FJ$. If $\Sigma_s \not\gg \max(c_{\rm left},c_{\rm right})$, one can still utilize the concept of the limiting current; however, then $I\neq FJ$, and the $i-j$ relation must be utilized.

In general, the two limiting currents are not equal (in the absolute sense) since they depend on the geometry and the left/right bulk concentrations. If either the geometry is asymmetric or the concentrations are asymmetric, so too will be the limiting currents. This is consistent with the $i-V$'s shown in main text Figure 3(a) and also in past works [16].

2. Over-limiting currents

For the case of symmetric concentrations, it is known that the current can surpass the theoretically predicted limiting current. However, for that to happen, additional physical mechanisms need to be added – like water splitting [19,20], surface conductance [21] and electro-convection [9,19,21–25]. Each of these mechanisms introduces a new term/equation or varies an existing term. All these variations, which are nonlinear, are essential components for the over-limiting currents.

B. Selectivity

In the main text, the counterionic transport number

$$\tau = \frac{j_+}{j_+ - j_-} = \frac{1}{2} + \frac{1}{2}\frac{Fj}{i} = \frac{1}{2} + \Delta\tau \,. \tag{S49}$$

serves as a proxy for "permselectivity" or, in short, "selectivity". The counterionic transport number can vary between the two extreme cases of $\tau = 1$ and $\tau = ½$. When $\tau = 1$, the system is ideally selective, whereby $j_- = 0$ (leading to complete exclusion of the negatively charged coions) and $j_+ = j = i/F$. If $\tau = ½$, the system is vanishingly selective, whereby the contribution of both species is identical, $j_+ = -j_-$, resulting in $j = 0$ and $i = 2Fj_+$. Here, the transport of coions is uninhibited.

This definition is the one used by the water desalination and energy harvesting communities. There is yet another definition for the word "selectivity", which is quite popular with the ion-channel and physiology community. Instead of using an absolute metric like the one here [Eq. (S49)], they have adopted a "relative metric", where one looks at the ratio of the absolute values of two different species, *m* and *n*, which can be either of the same or opposite signs. This ratio $|j_m / j_n|$ provides a relative metric of which species has a higher flux. While useful, one needs to acknowledge two advantages of Eq. (S49). First, it is an absolute metric. Second, this absolute metric appears in the resistance – in other words, it is naturally inherent to the system. These differences are elaborated in our two recent works [4,5], which go beyond the "simple" scenario of symmetric diffusion coefficients ($D_+ = D_-$) considered in this work (in [4,5], we consider $D_+ \neq D_-$).

One last comment regarding terminology is needed. Here, we have used the terms ideally and vanishingly selective systems. However, other names can be found [4,5]. The "vanishingly selectivity" is often termed as 'non-selective', 'vanishingly selective', 'poorly selective' [1,25], or 'bulk dominated'. Similarly, "ideal selectivity" also has various names, including 'highly

selective' [8,26], perfectly selective [1,25,27], 'ideally selective' [21,28,29], or the 'good coion exclusion limit' [30].

C. Proof that $R_{V=0}/R_{I=0} \le 1$

Since $R_{V=0}/R_{I=0} \le 1$ [Figure 6(b)] occurs at low concentrations (i.e., ideal selectivity wherein $\Sigma_s \gg c_{\text{left}}$ or $\tau = 1$), we restrict our discussion to this regime in which the two master equations can be reduced. Specifically, main text Eq. (14) can be reduced to $i = Fj$, while main text Eq. (7) is simplified such that [16]

$$V = \frac{c_{\text{bulk}}}{\Sigma_s} I R_2 + V_{\text{th}} \left(2 \ln \frac{V_{\text{th}} c_{\text{right}} + \frac{1}{2} c_{\text{bulk}} I \Sigma R_3}{V_{\text{th}} c_{\text{left}} - \frac{1}{2} c_{\text{bulk}} I \Sigma R_1} + \ln \frac{1}{C_r} \right). \tag{S50}$$

Utilizing the definition of the differential resistance, $R_{V=0} = (dV/dI)_{V=0}$ [main text Eq. (33)], yields

$$R = \frac{dV}{dI} = \frac{c_{\text{bulk}}}{\Sigma_s} R_2 + \frac{2V_{\text{th}}}{I} \left[\frac{1}{1 - c_{\text{bulk}} I \Sigma R_1 / (2 c_{\text{left}} V_{\text{th}})} - \frac{1}{1 + c_{\text{bulk}} I \Sigma R_3 / (2 c_{\text{right}} V_{\text{th}})} \right]. \tag{S51}$$

To compare this result with the results at $I = 0$, and to allow for a simple analysis, we shall now take the Taylor series of Eq. (S51)

$$R \approx \left[\frac{R_2}{\Sigma_s} + \frac{\Sigma R_1}{c_{\text{left}}} + \frac{\Sigma R_3}{c_{\text{right}}} \right] c_{\text{bulk}} + \left[\left(\frac{\Sigma R_1}{c_{\text{left}}} \right)^2 - \left(\frac{\Sigma R_3}{c_{\text{right}}} \right)^2 \right] \frac{c_{\text{bulk}}^2}{2V_{\text{th}}} I + O(I^2). \tag{S52}$$

The zeroth-order term, which is independent of the current, is the one that can be calculated from Eq. (18) in the limit of ideal selectivity. The second term in Eq. (S52) depends on an interplay of five parameters. Here, for simplicity, we focus the analysis on the situation considered in this work, wherein $\Sigma R_1 = \Sigma R_3$. If $C_r = c_{\text{right}}/c_{\text{left}} > 1$, the square bracketed term is positive, but $I_{V=0} < 0$ [main text Figure 7(b)], such that the second term is negative. However, if $C_r < 1$, the square bracketed term is negative with $I_{V=0} > 0$ [main text Figure 7(b)], such that the second term is negative. Thus, for $\Sigma R_1 = \Sigma R_3$, the second term in Eq. (S51) is always negative, meaning it reduces the resistance relative to the zeroth order term, such that $R_{V=0}/R_{I=0} \le 1$. In fact, it is easy to show that the differential resistance achieves a minimal value ($dR/dI = 0$) at $I_{R_{\min}} = V_{\text{th}} [c_{\text{left}}/(c_{\text{bulk}} \Sigma R_1) - c_{\text{right}}/(c_{\text{bulk}} \Sigma R_3)]$, which is independent of Σ_s. This minimal resistance is given by

$$R_{\min} = \frac{c_{\text{bulk}}}{\Sigma_s} R_2 + \frac{4 c_{\text{bulk}} \Sigma R_1 \Sigma R_3}{c_{\text{right}} \Sigma R_1 + c_{\text{left}} \Sigma R_3}. \tag{S53}$$

D. Non-rectangular geometries and multichannel systems

In this work, we have demonstrated that, in realistic systems, one must account for the effects of the microchannels, where the preferred scenario is the 1D nanoporous membrane interfacing with two large reservoirs (3L-1D). However, for the sake of fundamental sciences, one often prefers to use a nanochannel system (3L-2D or 3L-3D), where the nanochannel geometry need not be a rectangle. Ref. [18] showed how to modify the expressions for the nanochannel and field focusing resistances. However, since in this work, we give the final response in terms of the general term, our final expressions for the resistances and other characteristics remain unchanged.

Also, in contrast to this work, which considers a single nanochannel system, many works consider multichannel systems, which are supposedly not covered in this work. However, if the channels are equally spaced, one can use the approach suggested in our previous work [18], wherein the global geometry is divided by the number of channels into equal units, referred to as "unit-cells." The resistance, as well as the harvestable current and power, of each unit cell are described by the model presented in this work, such that the total resistance is divided by the number of unit cells (such as in a parallel circuit), and the current and power are multiplied by this number.

However, the final expressions, as given here in terms of the resistances, remain unchanged, such that this robust model extends beyond the simplified single-channel rectangular geometry and can describe multiple channels of arbitrary shape. Thus, we believe this model can be used by virtually all experimentalists and numerical scientists who consider more complex scenarios (multiple channels of arbitrary shape) than the simplified single-channel rectangular geometry.

SIV. NUMERICAL METHODS

A. Numerical Simulations.

The simulations were conducted in a non-dimensional formulation, following our past works [2,6,14,17], and the results were subsequently converted back to their dimensional form for presentation. To that end, we provide the non-dimensional form of the governing equations and boundary conditions [Eqs. (S1)-(S3), (S5)]. Thereafter, we will discuss the parameters. All dimensionless variables and parameters are denoted with tildes.

All concentrations were normalized by c_{left} (here, this is c_{bulk}), while the potential was normalized by V_{th}. The spatial variables (and derivatives) were normalized by L_2. The fluxes were normalized by Dc_{bulk}/L_2 and the space-charge density by Fc_{bulk}. Then the governing equations are

$$\tilde{\nabla}^2\tilde{\phi} = -\frac{\tilde{\rho}_e}{2\varepsilon^2} = -\frac{1}{2\varepsilon^2}(\tilde{c}_+ - \tilde{c}_- - \tilde{\Sigma}_s\delta_{2k}), \tag{S54}$$

$$-\tilde{\nabla}\cdot\tilde{\mathbf{j}}_+ = \tilde{\nabla}\cdot(\tilde{\nabla}c_+ + \tilde{c}_+\tilde{\nabla}\tilde{\phi}) = 0, \tag{S55}$$

$$-\tilde{\nabla}\cdot\tilde{\mathbf{j}}_- = \tilde{\nabla}\cdot(\tilde{\nabla}\tilde{c}_- - \tilde{c}_-\tilde{\nabla}\phi) = 0. \tag{S56}$$

Here, $\tilde{\varepsilon} = \lambda_D / L_2$ is the normalized Debye length [where, once more, $\lambda_D = \sqrt{\varepsilon_0\varepsilon_r \Re T / 2F^2 c_{\text{bulk}}}$, as given above in Sec. SI.B.], which is a bulk concentration-dependent quantity. The edge boundary conditions are

$$\tilde{c}_\pm(\tilde{x}=0) = 1 \quad , \quad \tilde{c}_\pm(\tilde{x}=\tilde{\Delta}_3) = \tilde{C}_r \quad , \quad \tilde{\phi}(\tilde{x}=0) = \tilde{V} \quad , \quad \tilde{\phi}(\tilde{x}=\tilde{\Delta}_3) = 0. \tag{S57}$$

These equations and boundary conditions are implemented in the finite elements program COMSOL™ using the Transport of Diluted Species and Electrostatics modules. The simulations were conducted following the approach used in our past works [2,6,14,17].

Figure S1 shows the considered 2D geometry, which is the side view of Figure 4 when $W_2 = W_1 = W_3$. In addition to these edge BCs, the no-flux conditions at the walls [Eq. (S16)] are also specified. Table S1 specifies all geometric parameters in their non-dimensional form, while Table S2 specifies all the required dimensional parameters.

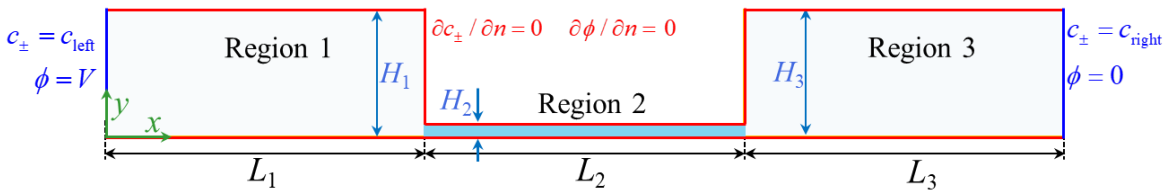

Figure S1. A 2D schematic representation of the side view of the geometry in main text Figure 4 with the boundary conditions. The height of the nanochannel, H_2, has been exaggerated for demonstration purposes.

Table S1. Non-dimensional geometric parameters for simulations.

Parameter	Value
Microchannel length, $\tilde{L}_{1,2,3}$	1
Microchannel heights, $\tilde{H}_{1,3}$	0.4
Nanochannel height, $\tilde{H}_2$	0.002 and 0.4

Table S2. Characteristic dimensional parameters used to move from non-dimensional formulation to dimensional formulation.

Parameter	Value
Nanochannel length, L_2 [mm]	1
Excess counterion concentration, Σ_s [mol/m^3]	1
KCl Diffusion coefficients, $D_{\pm}$ [m^2/s]	2×10^{-9}
Temperature, T [K]	298
Relative permittivity, ε_r	80

In a similar manner to how $\tilde{\varepsilon}$ is non-dimensional, so too is the parameter $\tilde{\Sigma}_s = \Sigma_s / c_{\text{bulk}}$. To vary the bulk concentrations in non-dimensional simulations, one needs to vary both $\tilde{\Sigma}_s$ and $\tilde{\varepsilon}$ simultaneously. To that end, when we varied $\tilde{\Sigma}_s$ from 10^{-3} to 10^{3} (with approximately 10 points per decade of $\tilde{\Sigma}_s$), we also modified $\tilde{\varepsilon}$ accordingly. To break the bulk concentration asymmetry, we considered $C_r = 10^{-1}, 1, 10$.

Finally, we scanned the non-dimensional voltage from $\tilde{V}_{\text{min}} = -10$ to $\tilde{V}_{\text{max}} = 10$ with jumps of $d\tilde{V} = 0.1$. In Comsol, we calculated $\tilde{J}$ and $\tilde{I}$ for our entire $\tilde{\Sigma}_s$ and $\tilde{V}$ range. The data was then post-processed (in Matlab). In Matlab, we first found the $\tilde{I}$ nearest to $\tilde{I} = 0$. Then, we interpolated between the five nearest points to find the $\tilde{I} = 0$ results shown in main text Figure 5 after proper re-dimensionalization. A similar process was conducted for $\tilde{V} = 0$ quantities. Since $\tilde{V} = 0$ was one of the pre-determined voltage drops, we were able to evaluate $\tilde{I}_{\tilde{V}=0}$ exactly at $\tilde{V} = 0$. To calculate $\tilde{R}_{\tilde{V}=0}$, we calculated the local slope between the five closest points to $\tilde{V} = 0$.

B. Numerical evaluation of transcendental equations

The $i - j$ equation [Eq. (S40)] is transcendental and cannot be solved analytically, such that numerical evaluation is required. The procedures used for their evaluations are now discussed. Importantly, all calculations from Eq. (S40) are considered in their non-dimensional form. Thereafter, all the calculations are transformed back to their dimensional form. For the sake of simplicity, in the following paragraphs, even though we consider the non-dimensional parameters, we will not add the tilde notations.:

1) $I = 0$: For $\hat{j}_{I=0}$, we solve main text Eq. (12) using a Newton-Raphson solver, where main text Eq. (21), $\hat{j}_{I=0} = 2D(\bar{S}_1 - \bar{S}_3)/L_2$, is used as the initial guess. The solver converged

quickly to the solution shown in Figure 5. Then $\hat{j}_{I=0}$ (or $\hat{J}_{I=0}$) is inserted into the remaining quantities ($\hat{V}_{I=0}$, τ and R_{Ohmic}).

2) $V=0$: We solve the $i-j$ relation [Eq. (S40)] for a wide range of values for j between the non-dimensional negative and positive limiting salt currents [Eq. (S48)]. The $i-j$ relation is solved using the 3rd order Householder method [31], with the initial guess of $i=1.01j$. After the root is found, the $i-j$ pair is inserted into the $V(i,j)$ [Eq. (S47)]. We then find the point nearest $V=0$ to find $i_{V=0}$. Also, using the five nearest points to $V=0$, we calculate the differential resistance $R_{V=0}=(dV/di)_{V=0}$. The $V=0$ solution for the one-layer system is substantially simpler and is covered extensively in Refs. [3–5].

REFERENCES

[1] R. Abu-Rjal, V. Chinaryan, M. Z. Bazant, I. Rubinstein, and B. Zaltzman, Effect of concentration polarization on permselectivity, Phys. Rev. E **89**, 012302 (2014).

[2] Y. Green, R. Abu-Rjal, and R. Eshel, Electrical resistance of nanochannel-microchannel systems: an exact solution, Phys. Rev. Appl. **14**, 014075 (2020).

[3] O. Lavi and Y. Green, A theoretical characterization of osmotic power generation in nanofluidic systems, Commun. Mater. **5**, 1 (2024).

[4] Y. Green, Universal Model for Ion Transport: Bridging The Goldman-Hodgkin-Katz Paradigm with Reverse Electrodialysis, Phys. Rev. Lett. **134**, 228401 (2025).

[5] Y. Green, Goldman-Hodgkin-Katz equation, reverse electrodialysis, and everything in between, Phys. Rev. E **111**, 064408 (2025).

[6] R. Abu-Rjal, Z. S. Siwy, and Y. Green, Electrical response of nanofluidic systems subjected to viscosity gradients, Phys. Rev. E **111**, (2025).

[7] I. Rubinstein, *Electro-Diffusion of Ions* (SIAM, 1990).

[8] I. Rubinstein and L. Shtilman, Voltage against current curves of cation exchange membranes, J. Chem. Soc. Faraday Trans. 2 **75**, 231 (1979).

[9] I. Rubinstein and B. Zaltzman, Electro-osmotically induced convection at a permselective membrane, Phys. Rev. E **62**, 2238 (2000).

[10] Y. Green, Effects of surface-charge regulation, convection, and slip lengths on the electrical conductance of charged nanopores, Phys. Rev. Fluids **7**, 013702 (2022).

[11] S. S. Dukhin, V. N. Shilov, and J. J. Bikerman, Dielectric Phenomena and Double Layer in Disperse Systems and Polyelectrolytes, J. Electrochem. Soc. **121**, 154C (1974).

[12] G. Yossifon, P. Mushenheim, Y.-C. Chang, and H.-C. Chang, Nonlinear current-voltage characteristics of nanochannels, Phys. Rev. E **79**, 046305 (2009).

[13] Y. Green, Current-voltage response for unipolar funnel-shaped nanochannel diodes, Phys. Rev. E **98**, 033114 (2018).

[14] Y. Green, S. Shloush, and G. Yossifon, Effect of geometry on concentration polarization in realistic heterogeneous permselective systems, Phys. Rev. E **89**, 043015 (2014).

[15] Y. Green and G. Yossifon, Effects of three-dimensional geometric field focusing on concentration polarization in a heterogeneous permselective system, Phys. Rev. E **89**, 013024 (2014).

[16] Y. Green, Y. Edri, and G. Yossifon, Asymmetry-induced electric current rectification in permselective systems, Phys. Rev. E **92**, 033018 (2015).

[17] Y. Green, R. Eshel, S. Park, and G. Yossifon, Interplay between Nanochannel and Microchannel Resistances, Nano Lett. **16**, 2744 (2016).

[18] J. Sebastian and Y. Green, Electrical Circuit Modeling of Nanofluidic Systems, Adv. Phys. Res. **2**, 2300044 (2023).

[19] M. B. Andersen, M. van Soestbergen, A. Mani, H. Bruus, P. M. Biesheuvel, and M. Z. Bazant, Current-Induced Membrane Discharge, Phys. Rev. Lett. **109**, 108301 (2012).

[20] C. P. Nielsen and H. Bruus, Transport-limited water splitting at ion-selective interfaces during concentration polarization, Phys. Rev. E **89**, 042405 (2014).

[21] E. V. Dydek, B. Zaltzman, I. Rubinstein, D. S. Deng, A. Mani, and M. Z. Bazant, Overlimiting Current in a Microchannel, Phys. Rev. Lett. **107**, 118301 (2011).

[22] S. M. Rubinstein, G. Manukyan, A. Staicu, I. Rubinstein, B. Zaltzman, R. G. H. Lammertink, F. Mugele, and M. Wessling, Direct Observation of a Nonequilibrium Electro-Osmotic Instability, Phys. Rev. Lett. **101**, 236101 (2008).

[23] G. Yossifon and H.-C. Chang, Selection of Nonequilibrium Overlimiting Currents: Universal Depletion Layer Formation Dynamics and Vortex Instability, Phys. Rev. Lett. **101**, 254501 (2008).

[24] S. J. Kim, Y.-C. Wang, J. H. Lee, H. Jang, and J. Han, Concentration Polarization and Nonlinear Electrokinetic Flow near a Nanofluidic Channel, Phys. Rev. Lett. **99**, 044501 (2007).

[25] I. Rubinstein and B. Zaltzman, Equilibrium Electroconvective Instability, Phys. Rev. Lett. **114**, 114502 (2015).

[26] O. Schnitzer and E. Yariv, Electric conductance of highly selective nanochannels, Phys. Rev. E **87**, 054301 (2013).

[27] N. Kavokine, R. R. Netz, and L. Bocquet, Fluids at the Nanoscale: From Continuum to Subcontinuum Transport, Annu. Rev. Fluid Mech. (2020).

[28] J. Schiffbauer and G. Yossifon, Role of electro-osmosis in the impedance response of microchannel-nanochannel interfaces, Phys. Rev. E **86**, 056309 (2012).

[29] E. Yariv, Asymptotic current-voltage relations for currents exceeding the diffusion limit, Phys. Rev. E **80**, 051201 (2009).

[30] M. Manghi, J. Palmeri, K. Yazda, F. Henn, and V. Jourdain, Role of charge regulation and flow slip in the ionic conductance of nanopores: An analytical approach, Phys. Rev. E **98**, 012605 (2018).

[31] Householder, *Numerical Treatment of a Single Nonlinear Equation*, First Edition (McGraw Hill Text, 1970).